International Journal of Plasticity 26 (2010) 516–532

Contents lists available at ScienceDirect

International Journal of Plasticity

journal homepage: www.elsevier.com/locate/ijplas

Anisotropic response of high-purity α-titanium: Experimental characterization and constitutive modeling

Michael E. Nixon [a], Oana Cazacu [b,*], Ricardo A. Lebensohn [c]

[a] Air Force Research Laboratory, Munitions Directorate, Eglin AFB, FL 32542, USA
[b] Department of Mechanical and Aerospace Engineering, University of Florida, REEF, 1350 N Poquito Road, Shalimar, FL 32539, USA
[c] Los Alamos National Laboratory, MST Division, Los Alamos, NM 87545, USA

ARTICLE INFO

Article history:
Received 28 May 2009
Received in final revised form 26 August 2009
Available online 8 September 2009

Keywords:
Twinning
α-Titanium
Tension–compression asymmetry
Orthotropic elasto-plastic model
Finite element

ABSTRACT

This paper presents a comprehensive experimental and theoretical investigation of the deformation behavior of high-purity, polycrystalline α-titanium under quasi-static conditions at room temperature. The initial material in this study was a cross-rolled plate with a strong basal texture. To quantify the plastic anisotropy and the tension–compression asymmetry of this material, monotonic tensile and compressive tests were conducted, on samples cut along different directions of the plate. A new anisotropic elastic/plastic model was developed to describe the quasi-static macroscopic response of the aggregate. Key in its formulation is the use of an anisotropic yield criterion that captures strength-differential effects and an anisotropic hardening rule that accounts for texture evolution associated to twinning. A very good agreement between FE simulations using the model developed and uniaxial data was obtained.

1. Introduction

Because of their outstanding engineering properties such as corrosion resistance, moderate weight (40% lighter than steel), and high strength, good formability, and biocompatibility, titanium and its alloys have found widespread use in high-performance applications. Examples include aircraft structures requiring greater heat resistance than aluminum alloys, aircraft engine applications, armor systems, etc. Considerable efforts have been devoted to the characterization and modeling of the response of titanium alloys (see for example, Follansbee et al., 1989; Lee and Lin, 1997; Nemat-Nasser et al., 2001; Picu and Majorell, 2002; Khan et al., 2004, 2007). The experimental data reported concerned mainly the uniaxial and torsional responses at different strain rates and temperatures, while data for non-proportional loading paths is rather limited (see Khan et al., 2007). Many studies have also been devoted to the understanding of the specific plastic deformation mechanisms at room temperature in pure titanium (e.g. Salem et al., 2003 for data on high-purity α-titanium; (Li et al., 1997 and Chun et al., 2005) for commercial purity titanium). Two types of deformation modes, slip and/or twinning, occur in titanium and its alloys during plastic deformation at room temperature. It is generally agreed that pronounced yield asymmetry is associated with the activation of twinning. Previous studies (Khan et al., 2007; Lee and Backofen, 1966; Kuwabara et al., 2001) have also shown that classic plasticity models, such as J_2 plasticity, or Hill (1948) are unable to capture this asymmetry that results from the combination of a sharp initial basal texture and the polarity of deformation twinning. Twinning plays two important roles in α-titanium. On the one hand, this deformation mechanism is a main contributor to texture evolution by reorienting the twinned areas (see Chun et al., 2005), even for the simplest monotonic loading paths. Furthermore, twinning drastically influences the strain-hardening behavior (see for example Salem et al., 2003). Accurate and realistic modeling of the behavior of α-titanium thus requires

* Corresponding author.
E-mail addresses: nixon@eglin.af.mil (M.E. Nixon), cazacu@reef.ufl.edu (O. Cazacu), lebenso@lanl.gov (R.A. Lebensohn).

0749-6419/$ - see front matter © 2009 Elsevier Ltd. All rights reserved.
doi:10.1016/j.ijplas.2009.08.007

incorporation of the effects of twinning on the mechanical response. Since, in crystal plasticity models, the distribution of crystal orientations in the given polycrystal, the available slip/twinning deformation systems, and the stress levels necessary to activate them are taken into account explicitly, the evolution of anisotropy due to texture development can be characterized by measuring the initial texture and updating the texture using a suitable model, e.g. homogenization schemes such as Taylor or the self-consistent model (see Hosford, 2005). Furthermore, the application of crystal plasticity models to hexagonal close-packed (HCP) materials and the incorporation of crystal plasticity calculations directly into multiscale finite element (FE) codes have received much attention lately. Models that account for both slip and twinning activity and employ Taylor (e.g. Staroselsky and Anand, 2003; Wu et al., 2007 or self-consistent, Tome and Lebensohn, 2004; Proust et al., 2007) averaging schemes to predict the aggregate behavior have been proposed. For example, Wu et al. (2007) concentrated their attention on the development of slip-hardening and twin-hardening functions based on the experimental data on high-purity titanium deformed in simple compression reported in Salem et al. (2003). These laws were incorporated into a Taylor crystal plasticity framework and further used to simulate the stress–strain response and texture evolution for monotonic loading (uniaxial compression and simple shear). However, no attempt was made either to predict the final deformed shape of the specimens, or to perform benchmark simulations of more complex monotonic loadings, such as bending. In Tome et al. (2001) a self-consistent viscoplastic model linked to the explicit FE code EPIC (Johnson et al., 2003) has been successfully used for describing the deformation of pure zirconium with a strong initial texture when subjected to quasi-static monotonic loading and bending, at room and liquid-nitrogen temperatures. The above direct implementation of a polycrystal model into a FE code, where a polycrystalline aggregate is associated with each FE integration point, has the advantage that it follows the evolution of anisotropy due to texture development. However, such FE calculations are computationally very intensive, thus limiting the applicability of these approaches to problems that do not require a fine spatial resolution.

An alternative promising approach is to develop anisotropic formulations at a macroscopic level that can be easily implemented in FE codes, and thus can be applied routinely for detailed analysis of complex forming processes. Unlike recent progress in the development of mathematical descriptions of anisotropic yield surfaces for materials with cubic crystal structure (for a review of such formulations see Cazacu and Barlat (2001), Cazacu and Barlat (2004) and Barlat et al. (2004)), macroscopic level modeling of yielding and strain-hardening of HCP materials is less developed. Some of the rigorous methods proposed to account for initial plastic anisotropy or to describe an average material response over a certain deformation range (see Barlat et al., 2007) can be extended to hexagonal materials. The major difficulty encountered in formulating analytic expressions for the yield functions of HCP metals is related to the description of the tension–compression asymmetry associated to twinning. Recently, yield functions in the three-dimensional stress space that describe both the tension–compression asymmetry and the anisotropic behavior of HCP metals have been developed. To describe yielding asymmetry that results either from twinning or from non-Schmid effects at single crystal level, Cazacu and Barlat (2004) have proposed an isotropic criterion expressed in terms of all invariants of the stress deviator. This isotropic yield criterion was applied to the description of crystal plasticity simulation results of Hosford and Allen (1973) and that of Vitek et al. (2004) for randomly oriented polycrystals (for more details, see Cazacu and Barlat, 2008). This isotropic criterion was further extended such as to incorporate anisotropy using the generalized invariants approach proposed by Cazacu and Barlat (2004). Comparison between this orthotropic criterion and data on magnesium and its alloys (Graff et al., 2007) and titanium (Cazacu and Barlat, 2004) show that this anisotropic model accurately describes both anisotropy and tension–compression asymmetry of these materials. In Cazacu et al. (2006) another isotropic pressure-insensitive yield criterion that accounts for yielding asymmetry between tension and compression associated with deformation twinning was developed. This isotropic criterion involves all principal values of the stress deviator. To account for both strength-differential effects and texture-induced anisotropy, an extension of this criterion using a fourth-order symmetric tensor operating on the Cauchy stress deviator was proposed by Cazacu et al. (2006). The orthotropic yield criterion of Cazacu et al. (2006) was shown to exhibit accuracy in describing the yield loci of magnesium (Cazacu et al., 2006) and titanium alloys (Cazacu et al., 2006; Khan et al., 2004, 2007).

The present study presents a comprehensive set of experiments aimed at understanding the response of high-purity α-titanium at room temperature, and a constitutive model to describe the observed behavior in the framework of anisotropic plasticity. We begin by reporting the results of a series of monotonic quasi-static tensile and compressive tests, conducted to quantify the plastic anisotropy and the tension–compression asymmetry of the material under investigation. The elastic/plastic anisotropic model developed for the description of the deformation behavior of this kind of material is then presented. The algorithmic aspects related to the implementation of the model developed in the FE code EPIC (Johnson et al., 2003) are also outlined. The ability of the proposed model to capture the main features of the observed behavior is next examined by comparing the experimental data with simulation results in terms of stress–strain response in uniaxial tensile and compression tests.

2. Experimental procedures

2.1. Material

The material used in this work was high purity (99.999%) titanium, purchased from Alpha Aesar of Johnson Matthey Electronics, Inc. (Spokane, WA). The material was supplied in the form of a 15.87 mm thick cross-rolled disk of 254 mm diameter. Optical microscopy showed that the as received material had equiaxed grains with an average grain size of about 20 μm (Fig. 1).

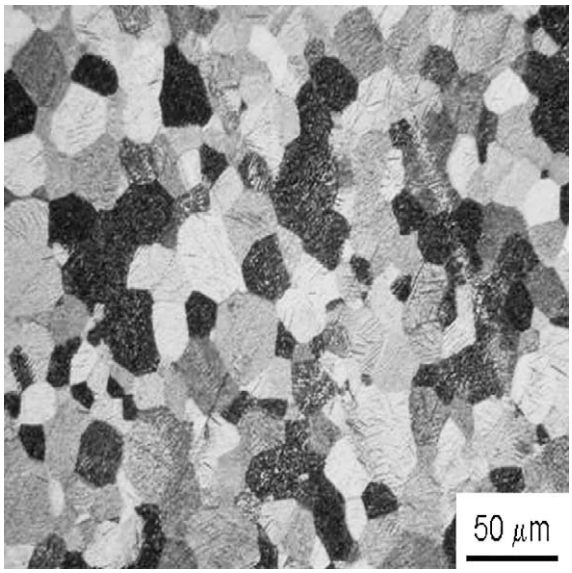

Fig. 1. Micrograph of the high-purity titanium plate material.

Twenty samples of approximate dimensions 19.05 mm × 19.05 mm × 15.87 mm were removed using water jet from the perimeter of the plate. Neighbor samples were separated by an angle of 11.32° (see Fig. 2). The basal plane (0001) pole figures of a few of these samples were measured by X-rays to confirm the orientation of the axes of orthotropy of the plate's texture. The basal plane aligns maximally in the normal-transverse plane at 30–40° from the plate normal direction (ND) towards the transverse direction (TD). This result was also confirmed by the analysis of the (0001) pole figures obtained from neutron diffraction measurements of the initial texture (see Fig. 3) carried out in the neutron time-of-flight (TOF) diffractometer High-Pressure-Preferred Orientation (HIPPO) at Los Alamos Neutron Science Center (LANSCE).

2.2. Quasi-static behavior of high-purity α-titanium

The quasi-static characterization tests consisted of uniaxial tension and compression tests that were conducted at room temperature and at a nominal strain rate of 0.001 s^{-1} using an Instron 1125 testing machine. Test specimens were cut from the plate using Electrical Discharge Machining (EDM) in order to eliminate artificial hardening that may occur using other

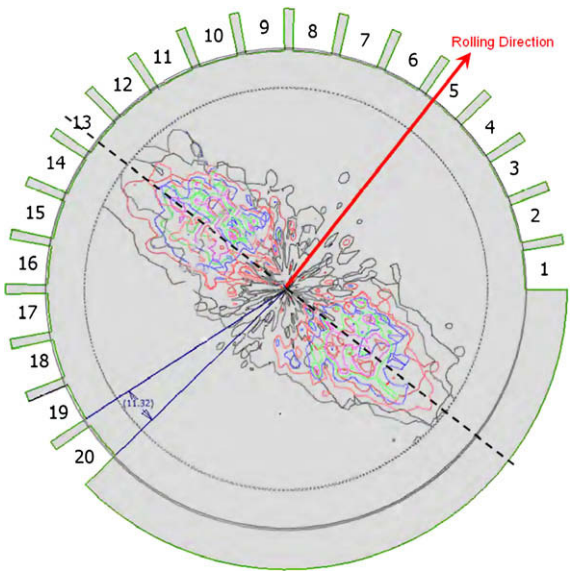

Fig. 2. Measured pole figure of the basal plane (0001); the rolling direction (RD) is indicated in red. (For interpretation of the references to color in this figure legend, the reader is referred to the web version of this paper.)

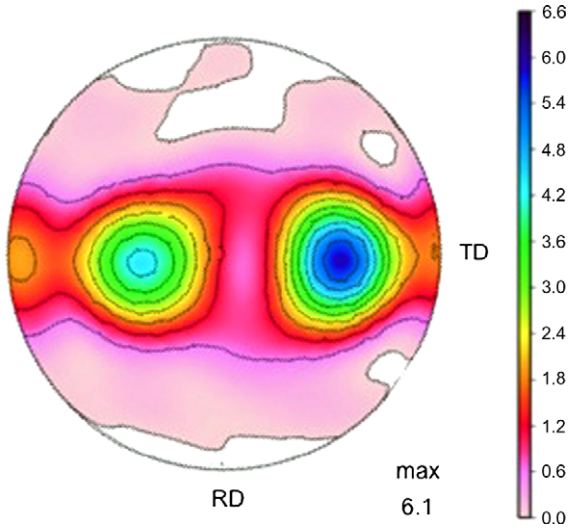

Fig. 3. (0001) pole figures measured by neutron diffraction showing the initial texture of the α-titanium plate used in this study. The rolling direction (RD) and transverse direction (TD) are in the plane of the disk, while the through-thickness (TT) direction is normal to the plate. Scale represents multiples of random distribution (mrd).

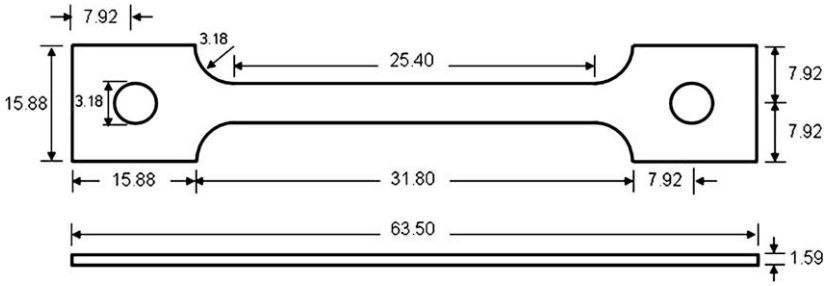

Fig. 4. Geometry and dimensions (in mm) of the specimens used for in-plane uniaxial tensile testing.

machining techniques. Tensile testing was carried out with a 5 kN load cell and an Instron model number G-51-12-A extensometer with a gauge length of 25.4 mm. To characterize the anisotropy of the material, standard tensile specimens were machined such the tensile direction was either parallel to the rolling direction (RD) or the transverse direction (TD) (see Fig. 4 for the dimensions of the samples). A specialized miniature test specimen was used for the through-thickness (TT) tensile tests (Fig. 5). The mini-tensile TT results may be affected by a 10% error, as demonstrated in a very recent paper by Kaschner et al. (in press).

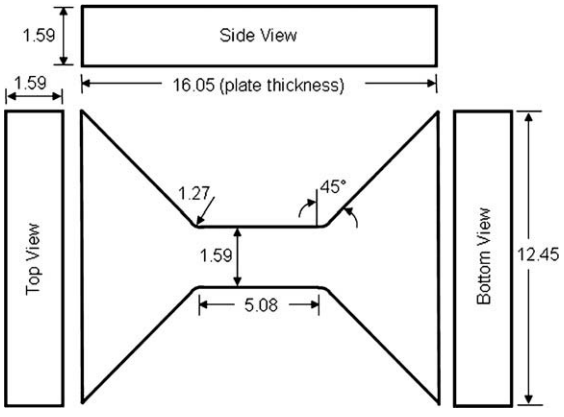

Fig. 5. Geometry and dimensions (in mm) of the through-thickness uniaxial tensile specimen.

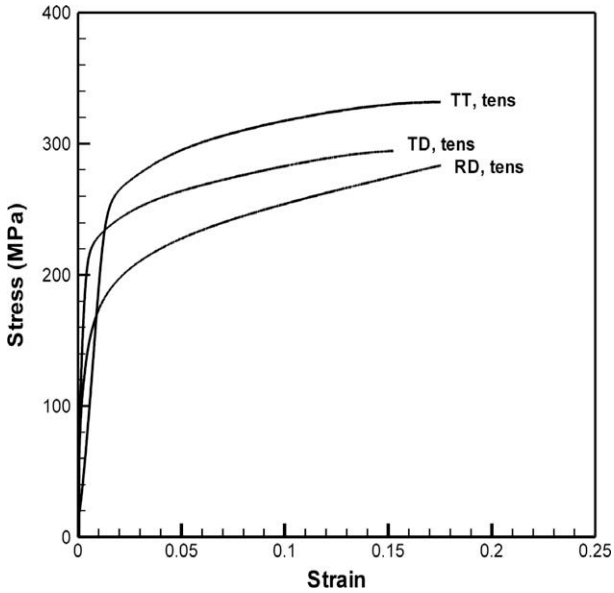

Fig. 6. Uniaxial tensile tests results along the rolling (RD), transverse (TD), and through-thickness direction (TT).

In order to examine the microstructural evolution, compression tests were carried out to approximatively 10%, 20%, 30%, 40% strains, respectively, or until complete failure of the specimen occurred. The uniaxial tensile test results (Figs. 6 and 7) show that the material displays orthotropic behavior. In tension, the material is weakest in the rolling direction and strongest in the through-thickness direction. In all tension tests, shear-type fracture was observed. In contrast, tensile fracture of magnesium alloy AZ31B, which also has HCP crystal structure is brittle (see data by Lou et al. (1997)).

To examine the effect of loading orientation on the mechanical response, cylindrical compression specimens (7.62 mm $\times$ 7.62 mm) were machined such that the axes of the cylinders were either along an in-plane (IP) or through-thickness (TT) plate directions. Compression testing was conducted using an Instron 100 kN load cell and an Instron extensometer model number G-51-17-A with a gauge length of 12.7 mm. In order to study the microstructural evolution with accumulated deformation, the uniaxial compression tests were conducted up to prestrain levels of 10%, 20%, 30% and 40%, respectively. In each test, the load was applied continuously (with no interruptions). To reduce the effects of friction, Molykote lubricant was

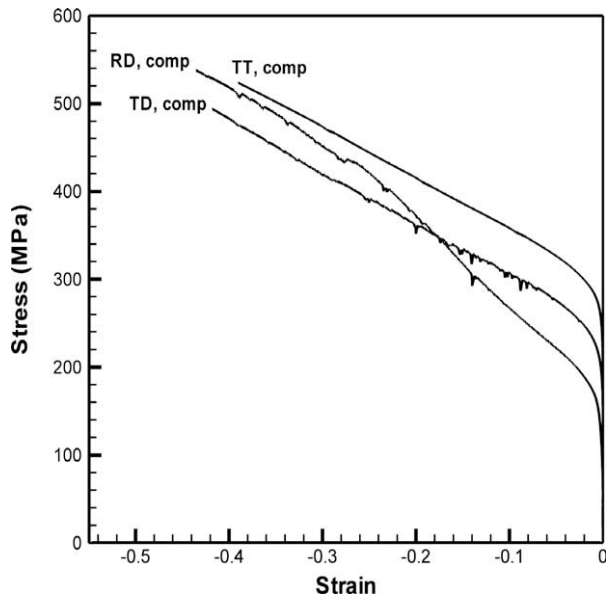

Fig. 7. Uniaxial compression tests results along the rolling (RD), transverse (TD), and through-thickness direction (TT).

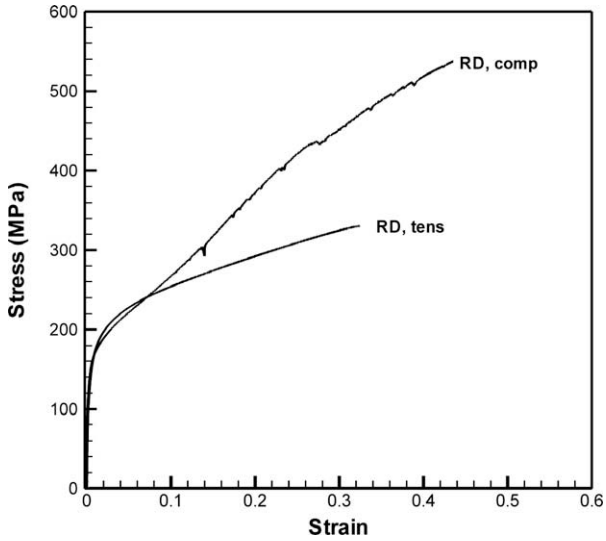

Fig. 8. Comparison between the compression and tension response in the rolling direction.

sprayed onto the platens prior to testing. Only minor barreling of the specimens was observed. The test results show that for this material the anisotropy in tension is more pronounced than the anisotropy in compression.

Comparison between compressive and tensile stress–strain response along the rolling direction is presented in Fig. 8. Although, initially there is no significant difference in yielding behavior (at 0.02% strain offset, the yield stress is 175 MPa), a very pronounced tension–compression asymmetry is observed after about 10% strain. Note the especially sharp difference in hardening evolution. While in tension, the material hardens gradually until plastic localization (diffuse necking) occurs at about 30% strain, in compression strain-hardening is strongly non-linear, with a very pronounced increase in hardening rate observed at about 10% strain. This change in hardening may be indicative of twinning. This hypothesis was verified by the analysis of the textures of the deformed specimen. The strong texture evolution resulting from large grain rotations associated with twinning is shown in Fig. 9 for samples deformed in compression to 10% and 40% strain, respectively.

A comparison of tension versus compression response along the transverse direction is shown in Fig. 10. Notice that the stress–strain curve in compression along the transverse direction does not show the features present in the stress–strain

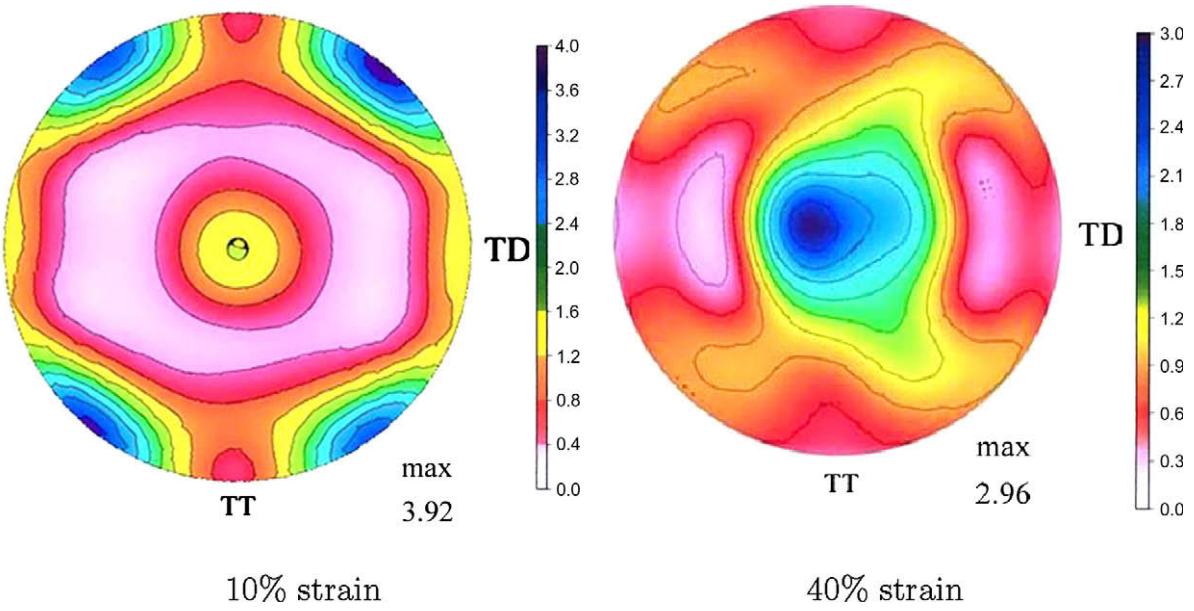

Fig. 9. (0001) pole figures for samples loaded in compression along the rolling direction. Scale represents multiples of random distribution (mrd).

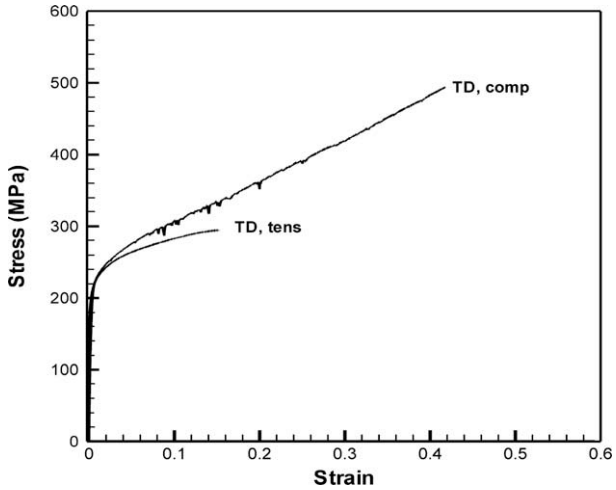

Fig. 10. Comparison between the compression and tension response in transverse direction.

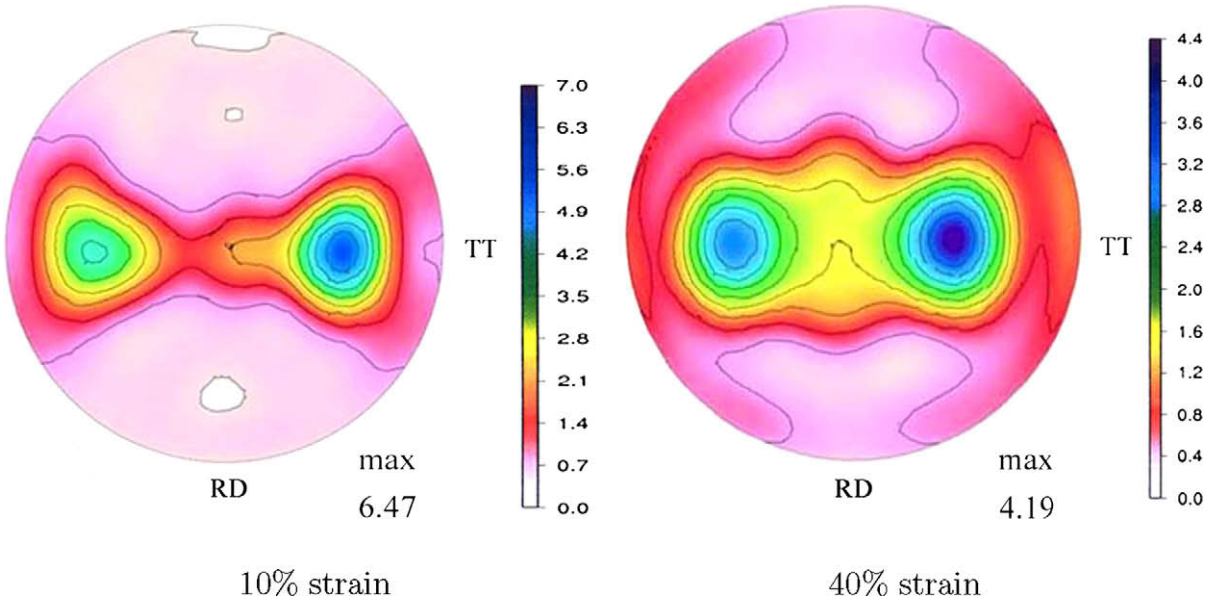

Fig. 11. (0001) pole figures for samples loaded in compression along the transverse direction. Scale represents multiples of random distribution (mrd).

response in the rolling direction compression. No significant change in work-hardening rate is observed in either compression or tension, which may be indicative of minimal deformation twinning. Indeed, post-test texture measurements of the specimen deformed to 10% and 40% strain in compression in the TD direction show little texture evolution, indicating that twinning is not a dominant deformation mechanism for this loading path (see Fig. 11).

Comparison between quasi-static test results in monotonic uniaxial compression and tension along the through-thickness direction are shown in Fig. 12. A strong tension/compression asymmetry in initial yielding is observed whereas the asymmetry in hardening evolution is less pronounced. Fig. 13 show post-test texture measurements for the TT specimen loaded in compression to 10% and 40% strain. Only a slight texture evolution is indicated.

3. Proposed elastic–plastic orthotropic model

To model the behavior of the high purity α-titanium material in the quasi-static loading regime, an elastic–plastic modeling approach is adopted. To describe the onset of yielding, an anisotropic yield criterion that captures both strength differential effects and the anisotropy in yielding is developed. A parameter identification procedure based on experimental

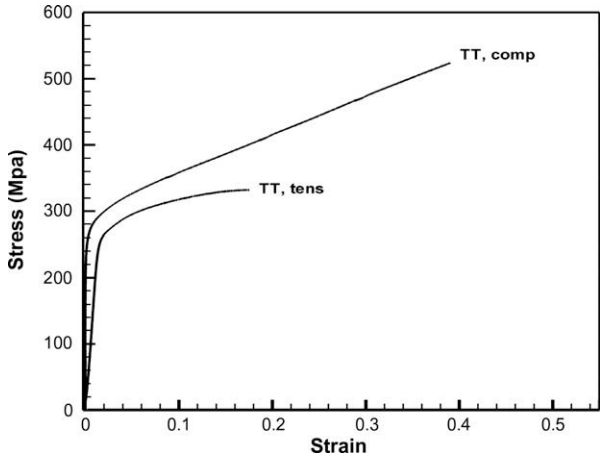

Fig. 12. Comparison between the compression and tension uniaxial response in the through-thickness direction.

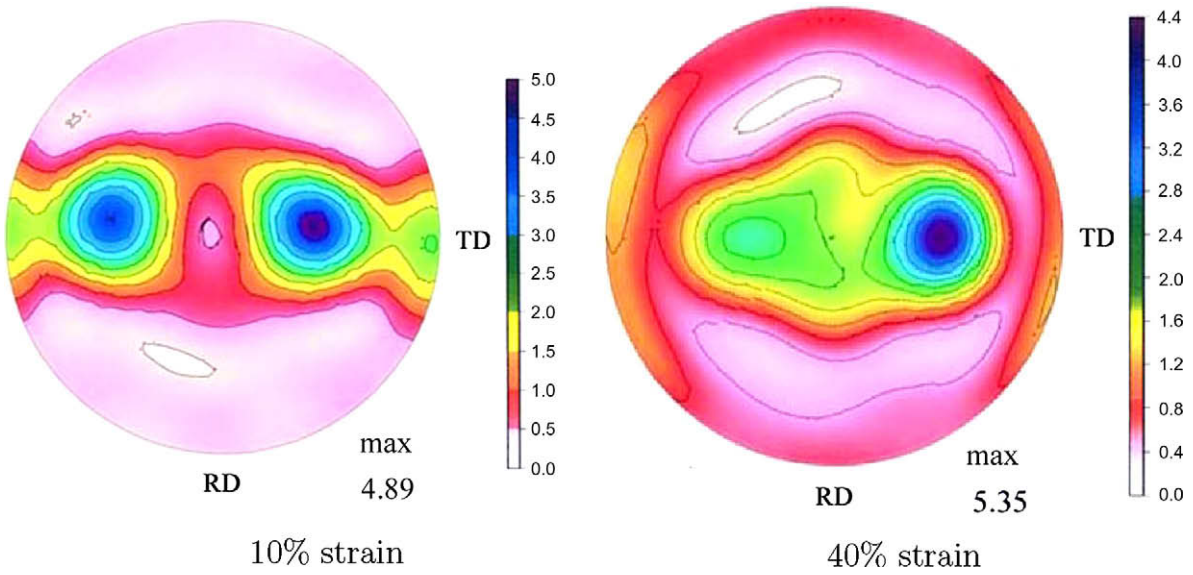

Fig. 13. (0001) pole figures for samples loaded in compression along the through thickness direction. Scale represents multiples of random distribution (mrd).

results is also outlined. The integration algorithm for the proposed model, and its implementation in the explicit FE code EPIC follows. We conclude with a comparison between model predictions and data in uniaxial tensile and compressive loading in various directions.

3.1. Proposed orthotropic yield criterion

One of the goals of this research is to advance the current state-of-the-art by developing user-friendly, micro-structurally based, and numerically robust macroscopic constitutive models that can capture with accuracy the particularities of the plastic response of hexagonal metals, in particular high purity α-titanium. A full three-dimensional orthotropic yield criterion is proposed. Key in this development is the use of the isotropic yield function developed by Cazacu and Barlat (2004) that captures tension/compression asymmetries. Thus, a brief overview of this isotropic yield criterion is first given.

If the deformation mechanism of plastic deformation is sensitive to the sign of the stress, as is the case of deformation twinning, the isotropic yield function ought to be represented by an odd function in the principal values of the stress deviator. To describe the asymmetry in yielding, due to twinning, Cazacu and Barlat (2004) proposed an isotropic yield criterion of the form

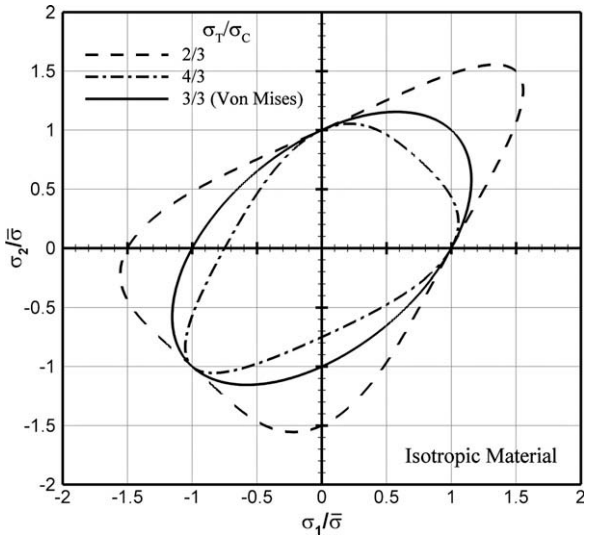

Fig. 14. Plane stress yield loci (3) for various values of the yield stress ratio σ_T/σ_C.

$$f(J_2,J_3) = J_2^{\frac{3}{2}} - cJ_3, \tag{1}$$

where c is a material parameter, $J_2 = \frac{1}{2}\mathrm{tr}(\boldsymbol{\sigma}'^2)$ and $J_3 = \frac{1}{3}\mathrm{tr}(\boldsymbol{\sigma}'^3)$ denote the second and third invariant of the stress deviator $\boldsymbol{\sigma}'$. The constant c can be expressed in terms of the yield in uniaxial tension, σ_T, and the yield in uniaxial compression, σ_C, as

$$c = \frac{3\sqrt{3}(\sigma_T^3 - \sigma_C^3)}{2(\sigma_T^3 + \sigma_C^3)} \tag{2}$$

If $\sigma_T = \sigma_C$ (no tension–compression asymmetry) then $c = 0$, and the isotropic criterion (1) reduces to the von Mises yield criterion. To ensure convexity, c is limited to the following range: $c \in \left[-3\sqrt{3}/2, 3\sqrt{3}/4\right]$. In principal stress space and for plane stress conditions ($\sigma_3 = 0$), the yield function (1) is expressed as

$$f(\sigma_1,\sigma_2) = \frac{1}{3}\left(\sigma_1^2 - \sigma_1\sigma_2 + \sigma_2^2\right)^{\frac{3}{2}} - \frac{c}{27}\left[2\sigma_1^3 + 2\sigma_2^3 - 3(\sigma_1+\sigma_2)\sigma_1\sigma_2\right] \tag{3}$$

When $c \neq 0$, Eq. (3) represents a triangle with rounded corners. As an example, in Fig. 14 is shown the yield locus (3) corresponding to three different ratios of σ_T/σ_C. When σ_T/σ_C is equal to unity, this isotropic yield locus reduces to the von Mises ellipse.

To describe both the asymmetry in yielding due to twinning and the anisotropy of rolled sheets, an extension to orthotropy of the isotropic criterion given by (1) is developed next. The extension to orthotropy will be done using a linear transformation approach. This approach (see for example, Barlat et al., 2007) consists in replacing in the expression of the isotropic criterion (1) the Cauchy stress, $\boldsymbol{\sigma}$, by $\boldsymbol{\Sigma} = \mathbf{L}\boldsymbol{\sigma}$, where $\mathbf{L}$ is a fourth order tensor. Let $J_2^\circ = \frac{1}{2}\mathrm{tr}(\Sigma^2)$ and $J_3^\circ = \frac{1}{3}\mathrm{tr}(\Sigma^3)$.

The proposed anisotropic criterion is of the form

$$f(J_2^\circ,J_3^\circ) = J_2^{\circ\frac{3}{2}} - cJ_3^\circ, \tag{4}$$

Thus the equivalent stress, $\bar{\sigma}$, associated to this orthotropic criterion is

$$\bar{\sigma} = A_1\left[(J_2^\circ)^{3/2} - cJ_3^\circ\right] \tag{5}$$

where A_1 is a constant defined such as $\bar{\sigma}$ reduces to the tensile yield stress in the rolling direction,

$$A_1 = 3\left[\left(a_2^2 + a_3^2 + a_2a_3\right)^{3/2} - c(a_2+a_3)a_2a_3\right]^{-1/3} \tag{6}$$

The tensor $\mathbf{L}$ satisfies: (a) the symmetry conditions: $L_{ijkl} = L_{jikl} = L_{jilk} = L_{klij}$ $(i,j,k,l = 1,\ldots,3)$, (b) the requirement of invariance with respect to the symmetry group of the material, and (c) $L_{1k} + L_{2k} + L_{3k} = 0$ for $k = 1$, 2, and 3, which ensures that $\boldsymbol{\Sigma}$ is traceless and consequently yielding is independent of hydrostatic pressure. Let $(\mathbf{x},\mathbf{y},\mathbf{z})$ be the reference frame associated with the material symmetries, with $\mathbf{x}$ designating the rolling direction, $\mathbf{y}$ the transverse direction, and $\mathbf{z}$ the thickness direction, respectively. Relative to the orthotropy axes $(\mathbf{x},\mathbf{y},\mathbf{z})$, $\mathbf{L}$ is represented by

$$\mathbf{L}=\begin{bmatrix} \frac{(a_2+a_3)}{3} & -\frac{a_3}{3} & -\frac{a_2}{3} & 0 & 0 & 0 \\ -\frac{a_3}{3} & \frac{(a_1+a_3)}{3} & -\frac{a_1}{3} & 0 & 0 & 0 \\ -\frac{a_2}{3} & -\frac{a_1}{3} & \frac{(a_1+a_2)}{3} & 0 & 0 & 0 \\ 0 & 0 & 0 & a_4 & 0 & 0 \\ 0 & 0 & 0 & 0 & a_5 & 0 \\ 0 & 0 & 0 & 0 & 0 & a_6 \end{bmatrix} \tag{7}$$

If the anisotropy of the material is fixed (i.e. the anisotropy of the material does not evolve with accumulated plastic strain) the coefficients a_i, $i = 1,\ldots,6$ are constants. In the symmetry reference frame, $(\mathbf{x},\mathbf{y},\mathbf{z})$, the generalized invariants, J_2° and J_3°, are expressed in terms of the components of the Cauchy stress $\boldsymbol{\sigma}$ as

$$\begin{aligned} J_2^\circ =& \frac{1}{9}\Big[(a_2^2+a_3^2+a_2a_3)\sigma_x^2+(a_1^2+a_3^2+a_1a_3)\sigma_y^2+(a_1^2+a_2^2+a_1a_2)\sigma_z^2+(-2a_3^2+a_1a_2-a_1a_3-a_2a_3)\sigma_x\sigma_y \\ &+(-2a_2^2-a_1a_2+a_1a_3-a_2a_3)\sigma_x\sigma_z+(-2a_1^2-a_1a_2-a_1a_3+a_2a_3)\sigma_y\sigma_z\Big]+a_4^2\tau_{xy}^2+a_5^2\tau_{xz}^2+a_6^2\tau_{yz}^2 \end{aligned} \tag{8}$$

$$\begin{aligned} J_3^\circ =& \frac{1}{27}\Big[(a_2^2a_3+a_2a_3^2)\sigma_x^3+(a_1^2a_3+a_3^2a_1)\sigma_y^3+(a_1^2a_2+a_1a_2^2)\sigma_z^3+(-a_1a_2^2+a_1a_3^2-a_2^2a_3-2a_2a_3^2)\sigma_x^2\sigma_y \\ &+(a_1a_2^2-a_1a_3^2-a_2^2a_3-2a_2a_3^2)\sigma_x^2\sigma_z+(-a_1^2a_2-a_1^2a_3+a_2a_3^2-2a_1a_3^2)\sigma_y^2\sigma_x+(a_1^2a_2-2a_1^2a_3-a_1a_3^2-a_2a_3^2)\sigma_y^2\sigma_z \\ &+(-a_1^2a_2-a_1^2a_3-2a_1a_2^2+a_2^2a_3)\sigma_z^2\sigma_x+(-2a_1^2a_2+a_1^2a_3-a_1a_2^2-a_2^2a_3)\sigma_z^2\sigma_y \\ &+2(a_1^2a_2+a_1^2a_3+a_2^2a_1+a_2^2a_3+a_3^2a_1+a_3^2a_2)\sigma_x\sigma_y\sigma_z\Big]+\frac{1}{3}\{[a_2a_4^2\sigma_x+a_1a_4^2\sigma_y-(a_1a_4^2+a_2a_4^2)\sigma_z]\tau_{xy}^2 \\ &+[a_3a_5^2\sigma_x-(a_1a_5^2+a_3a_5^2)\sigma_y+a_1a_5^2\sigma_z]\tau_{xz}^2+[(-a_2a_6^2-a_3a_6^2)\sigma_x-a_3a_6^2\sigma_y+a_2a_6^2\sigma_z]\tau_{yz}^2\}+2a_4a_5a_6\tau_{xy}\tau_{xz}\tau_{yz} \end{aligned} \tag{9}$$

These generalized invariants reduce to the isotropic invariants J_2 and J_3 when $\mathbf{L}$ is taken as the identity tensor so that $a_i = 1$ and $\boldsymbol{\Sigma} = \boldsymbol{\sigma}$. Thus, the proposed anisotropic criterion (5) involves seven parameters: the strength differential parameter c and the six anisotropy coefficients a_i. Of these six anisotropy coefficients, a_1 to a_4 are related to the in-plane properties of the sheet. These coefficients and c can be determined based on uniaxial tensile and compressive tests along different orientations θ with respect to the rolling direction $\mathbf{x}$. Let denote by σ_θ^T and σ_θ^C, the normalized uniaxial flow stress data normalized by the tensile yield stress in the rolling direction.

In particular, according to (5)

$$\sigma_o^C=\frac{1}{A_1}\left\{(a_2^2+a_3^2+a_2a_3)^{\frac{3}{2}}+c(a_2^2a_3+a_3^2a_2)\right\}^{-\frac{1}{3}} \tag{10}$$

Similarly, the proposed yield criterion predicts that the tensile yield stress and compressive yield stress along the transverse direction $\mathbf{y}$ are

$$\sigma_{90}^T=\frac{1}{A_1}\left\{(a_1^2+a_3^2+a_1a_3)^{\frac{3}{2}}-c(a_1^2a_3+a_3^2a_1)\right\}^{-\frac{1}{3}} \tag{11}$$

$$\sigma_{90}^C=\frac{1}{A_1}\left\{(a_1^2+a_3^2+a_1a_3)^{\frac{3}{2}}+c(a_1^2a_3+a_3^2a_1)\right\}^{-\frac{1}{3}} \tag{12}$$

Using (5), we obtain that the tensile yield stress and compressive yield stress along the through-thickness direction $\mathbf{z}$ are

$$\sigma_z^T=\frac{1}{A_1}\left\{(a_1^2+a_2^2+a_1a_2)^{\frac{3}{2}}-c(a_1^2a_2+a_2^2a_1)\right\}^{-\frac{1}{3}} \tag{13}$$

$$\sigma_z^C=\frac{1}{A_1}\left\{(a_1^2+a_2^2+a_1a_2)^{\frac{3}{2}}+c(a_1^2a_2+a_2^2a_1)\right\}^{-\frac{1}{3}} \tag{14}$$

When $\sigma_1=\sigma_2=\sigma_b^T$ and $\sigma_3=0$ (equibiaxial loading), according to the proposed criterion yielding occurs when

$$\sigma_b^T=\frac{1}{A_1}\left[(2a_1-2b_2-b_3)^{3/2}-c\frac{a_1a_2(a_1+a_2)}{27}\right]^{-\frac{1}{3}} \tag{15}$$

while under equibiaxial compression, i.e. for $\sigma_1=\sigma_2=\sigma_b^C$

$$\sigma_b^C=\frac{1}{A_1}\left[(2a_1-2b_2-b_3)^{3/2}+c\frac{a_1a_2(a_1+a_2)}{27}\right]^{-\frac{1}{3}} \tag{16}$$

Furthermore, we assume that the plastic potential coincides with the yield function. Let denote by r_θ^T and r_θ^C the Lankford coefficients (width to thickness strain ratios) under uniaxial tension and uniaxial compression in a direction at angle θ with the rolling direction $\mathbf{x}$, respectively. According to the proposed orthotropic criterion, it follows that:

$$3\left[r_0^T(3\alpha_1+\alpha_2-\alpha_3)-(\alpha_3-\alpha_1-\alpha_2)\right]\sqrt{\alpha_1}-2c\left[(3\beta_1-\beta_3)r_0^T-\beta_3\right]=0 \tag{17}$$

$$3\left[r_0^C(3\alpha_1+\alpha_2-\alpha_3)-(\alpha_3-\alpha_1-\alpha_2)\right]\sqrt{\alpha_1}+2c\left[(3\beta_1-\beta_3)r_0^C-\beta_3\right]=0 \tag{18}$$

$$3\left[r_{90}^T(3\alpha_2+\alpha_1-\alpha_3)-(\alpha_3-\alpha_1-\alpha_2)\right]\sqrt{\alpha_2}-2c\left[(3\beta_2-\beta_4)r_{90}^T-\beta_3\right]=0 \tag{19}$$

$$3\left[r_{90}^C(3\alpha_2+\alpha_1-\alpha_3)-(\alpha_3-\alpha_1-\alpha_2)\right]\sqrt{\alpha_2}+2c\left[(3\beta_2-\beta_4)r_{90}^C-\beta_3\right]=0 \tag{20}$$

where the superscripts T and C designate tensile and compressive states, respectively. The constants α_i, $i=1,\ldots,3$ and β_j, $j=1,\ldots,4$ are expressed in terms of the anisotropy coefficients as

$$\begin{aligned}
\alpha_1 &= \frac{1}{9}(a_2^2+a_3^2+a_2a_3)\\
\alpha_2 &= \frac{1}{9}(a_1^2+a_3^2+a_1a_3)\\
\alpha_3 &= \frac{1}{9}(a_1^2+a_2^2+a_1a_2)\\
\beta_1 &= \frac{a_2a_3}{27}(a_2+a_3)\\
\beta_2 &= \frac{a_1a_3}{27}(a_1+a_3)\\
\beta_3 &= \beta_1+\frac{1}{27}(a_3^2a_2+a_2^2a_1-a_3^2a_1)\\
\beta_4 &= \beta_2+\frac{1}{27}(a_3^2a_1+a_2^2a_1-a_3^2a_2)
\end{aligned} \tag{21}$$

In conclusion, using the above equations with $a_1=1$, the coefficients a_i, $i=2,\ldots,4$ and the strength parameter c can be determined by minimizing an error function of the form

$$E(a_2,a_3,a_4,c)=\sum_j w_j\left(\frac{\sigma_\theta^T}{\sigma_\theta^{\exp}}-1\right)^2+\sum_k w_k\left(\frac{\sigma_\theta^C}{\sigma_\theta^{\exp}}-1\right)^2+\sum_{jj} w_{jj}\left(\frac{r_\theta^T}{r_\theta^{\exp}}-1\right)^2+\sum_{kk} w_{kk}\left(\frac{r_\theta^C}{r_\theta^{\exp}}-1\right)^2 \tag{22}$$

where j is the number of experimental tensile yield stresses, jj is the number of experimental tensile Lankford coefficients, k is the number of experimental compressive yield stresses, kk is the number of experimental compressive Lankford coefficients while w_j, w_k, w_{jj} and w_{kk} are weights given to the respective experimental values. The theoretical values are calculated according to the above equations. The remaining anisotropy coefficients, a_5 and a_6, which are associated with out-of-plane properties may be determined based on out-of-plane data such as yield stress for simple shear in the (**y,z**) and (**z,x**) planes, respectively. Generally, if experimental data are not available for a given strain path, they can be substituted with numerical data obtained from polycrystalline calculations.

3.2. Modeling anisotropic hardening due to evolving texture

Previous experimental observations on hardening of hexagonal materials (e.g. Hosford and Allen, 1968; Lee and Backofen, 1966; Lou et al., 1997) as well as the quasi-static monotonic data on α-titanium reported in this paper (see Section 2.2) show that the hardening rate is strongly dependent not only on the loading path but also on the sense of loading. Thus, the directionality of hardening cannot be neglected even for the simplest loading conditions such as monotonic loading. This anisotropic hardening, which is due to evolving texture, cannot be described using classical isotropic or kinematic hardening laws.

A general methodology for the description of yielding anisotropy and its evolution with accumulated deformation for both quasi-static and dynamic loading conditions have been proposed by Plunkett et al. (2006) and Plunkett and Cazacu (2008). The anisotropy coefficients as well as the size of the elastic domain were considered to be functions of the equivalent plastic strain associated with Cazacu et al. (2006) orthotropic yield criterion. Experimental measurements and/or polycrystalline calculations were used to calculate the flow stress in various stress directions for a finite set of values of the equivalent plastic strain. Next, an interpolation technique was used to construct subsequent yield surfaces. Another method, which consists in determining explicit analytic expressions for the laws of variation of the anisotropy coefficients with accumulated plastic deformation was proposed by Graff et al. (2007) and used in conjunction with the orthotropic yield criterion of Cazacu and Barlat (2004) for the description of the anisotropy in yielding due to texture evolution in magnesium. However, the determination of these analytic laws of variation for the anisotropy coefficients and strength differential parameter requires a large amount of data. In this paper, we use the methodology of Plunkett et al. (2006) in conjunction with the new orthotropic yield criterion (5). The hardening variable is considered to be the equivalent plastic strain $\bar{\varepsilon}_p$ associated with this effective stress through the work-equivalence principle. Thus, from experimental and/or numerical results from polycrystal calculations, we determine the anisotropic coefficients a_i and c for a finite set of values of the equivalent plastic strain, say $\bar{\varepsilon}_p^1<\bar{\varepsilon}_p^2<\cdots<\bar{\varepsilon}_p^m$, and calculate for each of the individual strain level $\bar{\varepsilon}_p^j$, $j=1,\ldots,m$, the effective stress $\bar{\sigma}^j=\bar{\sigma}\left\{\boldsymbol{\sigma},L\left(\bar{\varepsilon}_p^j\right),c\left(\bar{\varepsilon}_p^j\right)\right\}$, using (5) as well as $Y^j=Y\left(\bar{\varepsilon}_p^j\right)$, where Y is the effective stress-effective plastic strain function in

the tensile rolling direction. Then, an interpolation procedure is used to obtain the yield surfaces corresponding to any given level of accumulated strain. Thus, for a given arbitrary $\bar{\epsilon}_p$, the anisotropic yield function is of the form

$$Q(\boldsymbol{\sigma}, \bar{\epsilon}_p) = \Gamma(\boldsymbol{\sigma}, \bar{\epsilon}_p) - \Pi(\bar{\epsilon}_p) \tag{23}$$

with

$$\Gamma(\boldsymbol{\sigma}, \bar{\epsilon}_p) = \xi(\bar{\epsilon}_p)\bar{\sigma}^j + (1 - \xi(\bar{\epsilon}_p))\bar{\sigma}^{j+1} \tag{24}$$

and

$$\Pi(\boldsymbol{\sigma}, \bar{\epsilon}_p) = \xi(\bar{\epsilon}_p)Y^j + (1 - \xi(\bar{\epsilon}_p))Y^{j+1} \tag{25}$$

for any $\bar{\epsilon_p}^j \leqslant \bar{\epsilon}_p \leqslant \bar{\epsilon_p}^{j+1}$, $j = 1, \ldots, m-1$. For linear interpolation, the weighting parameter $\xi(\bar{\epsilon}_p)$ appearing in Eqs. (24) and (25) is defined as:

$$\xi(\bar{\epsilon}_p) = \frac{\bar{\epsilon}_p^{j+1} - \bar{\epsilon}_p}{\bar{\epsilon}_p^{j+1} - \bar{\epsilon}_p^{j}} \tag{26}$$

such that $\xi\left(\bar{\epsilon}_p^j\right) = 1$ and $\xi\left(\bar{\epsilon}_p^{j+1}\right) = 0$. By considering that the anisotropy coefficients a_j, $j = 1, \ldots, 6$, and the strength differential parameter c evolve with the plastic deformation, the observed distortion and change in shape of the yield loci of hcp materials could be captured. Obviously, if these coefficients are taken constant, the proposed hardening law reduces to the classic isotropic hardening law, the shape of the yield locus depends only on the initial texture and does not change.

4. Application of the proposed model to α-titanium

In this section, we apply the proposed model to the description of the anisotropy and asymmetry in yielding of the α-titanium plate material studied. The r-values were not measured. The experimental data used in the error function (22) consist of the measured tensile and compressive flow data in the RD, TD, and TT directions. Equal weights were given to the experimental data. The parameter a_1 is set equal to unity while the numerical values of the anisotropy coefficients a_2 to a_4 corresponding to fixed levels of accumulated plastic strain $\bar{\epsilon}_p$ are given in Table 1. No data were available for determination of the coefficients a_5 and a_6. Their values were set equal to the isotropic values (i.e. unity). The corresponding theoretical biaxial plastic potential curves along with the experimental values (represented by symbols) are shown in Fig. 15. Note that the proposed criterion matches the data well.

Note that for strains below 10% strain, the predicted yield loci have an elliptical type shape, which is typical for slip dominated plastic deformation. Beyond this strain level, the model predicts that the yield loci have a triangular shape and that the tension–compression asymmetry is very pronounced. It is worth noting that this change in shape occurs at the strain level associated with twin activation in the rolling direction. Hill (1948) is the most widely used orthotropic yield criterion available and has proven to be accurate and robust for many materials, especially steels. However, it cannot account for the strength differential observed in hexagonal materials. For comparison purposes, Hill's criterion is applied to the high purity titanium material. With respect to the orthotropy axes (x, y, z), Hill (1948) orthotropic yield criterion is written as

$$F(\sigma_y - \sigma_z)^2 + G(\sigma_z - \sigma_x)^2 + H(\sigma_x - \sigma_y)^2 + 2L\tau_{yz}^2 + 2M\tau_{zx}^2 + 2N\tau_{xy}^2 = 1 \tag{27}$$

where the coefficients F, G, H, L, M, and N are material constants.

The coefficients F, G, and H were calculated using the analytic expressions of these coefficients in terms of the flow stresses along the axes of symmetry of the material (see Hill, 1948). The numerical values for the high-purity titanium are: $F = 4.147\ \text{MPa}^{-1}$, $G = 4.726\ \text{MPa}^{-1}$ and $H = 6.986\ \text{MPa}^{-1}$. In Fig. 16 are shown the theoretical yield loci according to Hill (1948) along with the yield loci predicted by the anisotropic model at a strain of 20%. Note that Hill's, 1948 criterion cannot capture the observed behavior while the proposed model describes very well the pronounced strength differential effects displayed by the material.

The developed orthotropic yield criterion in conjunction with the anisotropic hardening law presented in the previous section and associated flow rule was implemented into the explicit FE code EPIC (Johnson et al., 2003). General aspects

Table 1
Yield function (5) coefficients for high-purity α-titanium corresponding to fixed values of the equivalent plastic strain $\bar{\epsilon}_p$. Note a_1 is set to 1 for all cases.

$\bar{\epsilon}_p$	a_2	a_3	a_4	c
0.000	0.9186	1.9985	1.3286	−0.3975
0.025	0.9071	1.7270	1.3972	−0.4202
0.050	0.8343	1.6477	1.3651	−0.3422
0.075	0.8576	1.6193	1.4135	−0.3746
0.100	0.8902	1.6062	1.4490	−0.5142
0.200	0.9443	1.4246	1.4262	−9.6852

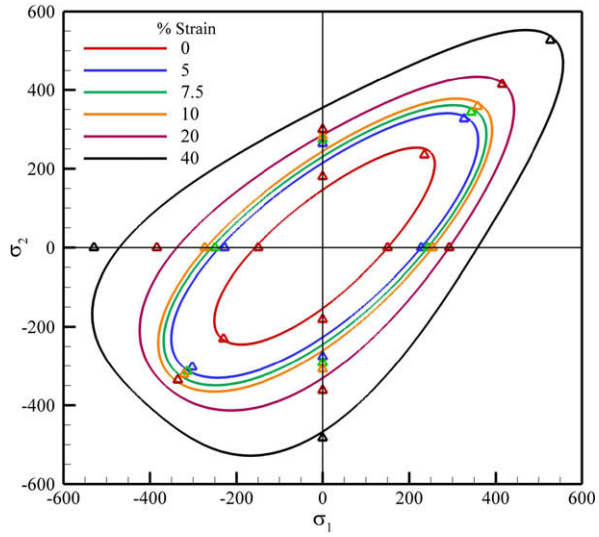

Fig. 15. Theoretical plastic potential according to (5) and experimental data (symbols) corresponding to fixed values of the equivalent plastic strain $\bar{\epsilon}_p$. Stresses are in MPa.

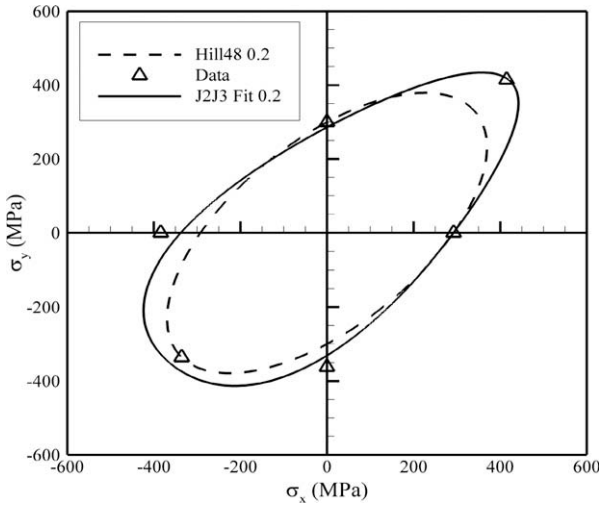

Fig. 16. Theoretical yield loci according with Hill (1948) criterion and the proposed criterion (5) in comparison with experimental flow stresses (symbols) on high-purity α-titanium for 20% pre-strain.

related to the solution of the plastic corrector problem are presented in what follows. The elastic strains are usually much smaller than plastic strains, hence an additive decomposition of the total strain rate $\dot{\epsilon}$ into an elastic part $\dot{\epsilon}_e$ and a plastic part $\dot{\epsilon}_p$ is generally considered. The elastic stress–strain relationship is given by

$$\dot{\boldsymbol{\sigma}} = \mathbf{C}\dot{\boldsymbol{\epsilon}}_e \tag{28}$$

where $\mathbf{C}$ denotes the fourth-order elasticity tensor.

The equivalent stress $\bar{\sigma}$ is given by (5) and the evolution of the plastic strain by an associated flow rule:

$$\dot{\boldsymbol{\epsilon}}_p = \dot{\lambda}\frac{\partial\bar{\sigma}}{\partial\boldsymbol{\sigma}} \tag{29}$$

Since the effective stress $\bar{\sigma}$ is a first-order homogeneous function in stresses (see (5)), from the work-equivalence principle follows that the law of evolution of the hardening variable $\bar{\epsilon}_p$ is: $\dot{\bar{\varepsilon}}_p = \dot{\lambda}$. Enforcing the Kuhn–Tucker loading–unloading conditions, follows that the tensor of tangent elastoplastic moduli, $\mathbf{C}^{\mathrm{ep}}$, that relates the current stress increment to the current total stress increment is given by:

$$\mathbf{C}^{\mathrm{ep}} = \begin{cases} \mathbf{C} & \text{for } \dot{\lambda} = 0 \\ \mathbf{C} - \frac{\mathbf{C}:\frac{\partial \Gamma}{\partial \boldsymbol{\sigma}} \otimes \mathbf{C}:\frac{\partial \Gamma}{\partial \boldsymbol{\sigma}}}{\frac{\partial \Gamma}{\partial \boldsymbol{\sigma}}:\mathbf{C}:\frac{\partial \Gamma}{\partial \boldsymbol{\sigma}} + \frac{\partial \Pi}{\partial \bar{\epsilon}_p}\frac{\partial \Gamma}{\partial \bar{\epsilon}_p}} & \text{for } \dot{\lambda} > 0 \end{cases} \tag{30}$$

where

$$\frac{\partial \Gamma}{\partial \boldsymbol{\sigma}} = \xi(\bar{\epsilon}_p)\frac{\partial \bar{\sigma}^j}{\partial \boldsymbol{\sigma}} + (1 - \xi(\bar{\epsilon}_p))\frac{\partial \bar{\sigma}^{j+1}}{\partial \boldsymbol{\sigma}} \tag{31}$$

$$\frac{\partial \Gamma}{\partial \bar{\epsilon}_p} = \frac{\bar{\sigma}^{j+1} - \bar{\sigma}^j}{\bar{\epsilon}_p^{j+1} - \bar{\epsilon}_p^j} \tag{32}$$

$$\frac{\partial \Pi}{\partial \bar{\epsilon}_p} = \frac{Y^{j+1} - Y^j}{\bar{\epsilon}_p^{j+1} - \bar{\epsilon}_p^j} \tag{33}$$

In displacement-based FE formulations, for a prescribed nodal displacement, at each Gauss point the system of Eqs. (28) and (29) are integrated to update the stress and hardening parameter. We use the convex cutting plane algorithm (Simo and Hughes, 1998). During a time step $[t_n, t_{n+1}]$, a trial elastic stress is computed by making use of the elastic stress–strain relation (28), i.e. $\sigma_{n+1}^{\mathrm{trial}} = \sigma_n + \mathbf{C} : \Delta\varepsilon_n$. Next, the generalized invariants of $\sigma_{n+1}^{\mathrm{trial}}$ are calculated. If $Q(\sigma_{n+1}^{\mathrm{trial}}, \bar{\varepsilon}_n^p) = \Gamma(\sigma_{n+1}^{\mathrm{trial}}, \bar{\varepsilon}_n^p) - \Pi(\bar{\varepsilon}_n^p) \leqslant 0$, then the process is elastic and the trial state is the final state. If, on the other hand, $\Gamma(\sigma_{n+1}^{\mathrm{trial}}, \bar{\varepsilon}_n^p) - \Pi(\bar{\varepsilon}_n^p) > 0$, the Kuhn–Tucker conditions are violated by the trial state which lies outside the yield surface. Consistency is restored by a return mapping algorithm. Basically, the constraint equation

$$\begin{aligned} F_{n+1} &= \Gamma(\sigma_{n+1}, \bar{\varepsilon}_n^p + \Delta\lambda) - \Pi(\bar{\varepsilon}_n^p + \Delta\lambda) = 0 \\ \sigma_{n+1} &= \sigma_{n+1}^{\mathrm{trial}} - \Delta\lambda \mathbf{C} : \left(\frac{\partial Q}{\partial \boldsymbol{\sigma}}\right) \end{aligned} \tag{34}$$

is linearized and the increment to the plastic multiplier is computed. The stresses, strains, and equivalent strain are updated and the yield criterion should be satisfied within a specified tolerance. If this tolerance has not been met, the plastic corrector step is repeated until convergence is obtained. Once this happens, the updated stresses and strains are accepted as the current state.

For uniaxial loading conditions, the simulations involved a single element with eight nodes with a single integration point. The cell was stretched uniaxially and the obtained stress versus strain results were compared to the appropriate experimental data. For each simulation, four nodes on one face of the element were restrained and the four nodes on the opposite face were given a constant velocity in either the tensile or compressive direction.

The simulated normal stresses in the appropriate loading direction versus the effective strain are compared to the corresponding experimental data (see Figs. 17–19). Note that the model accurately reproduces the data for each loading condition.

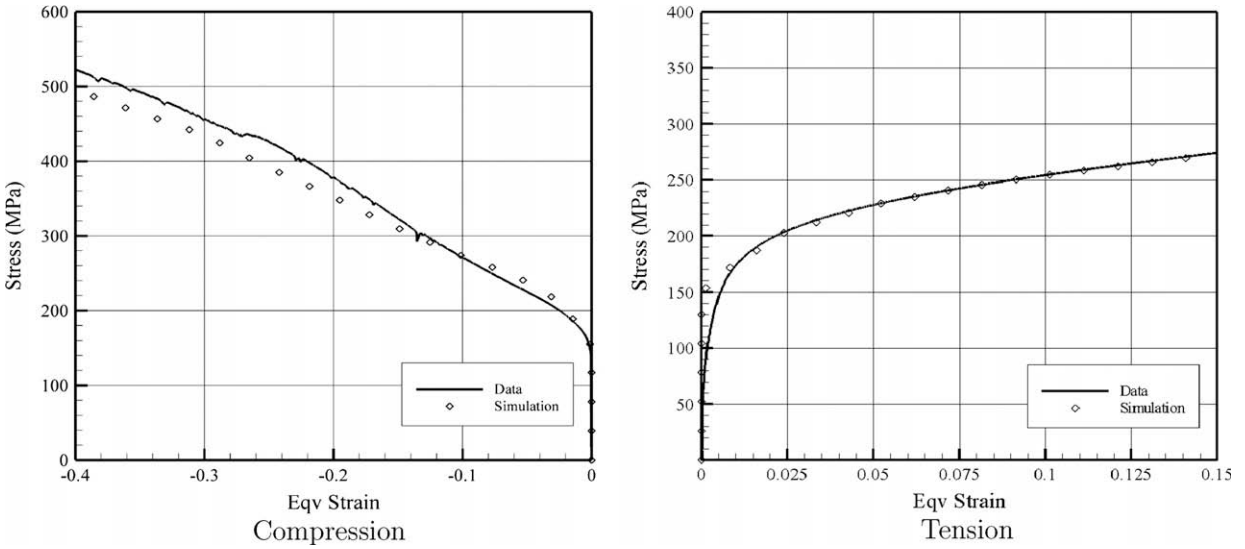

Fig. 17. Comparison between finite element simulation results using the proposed model and experimental data corresponding to uniaxial loading in the rolling direction. Symbols are simulation results.

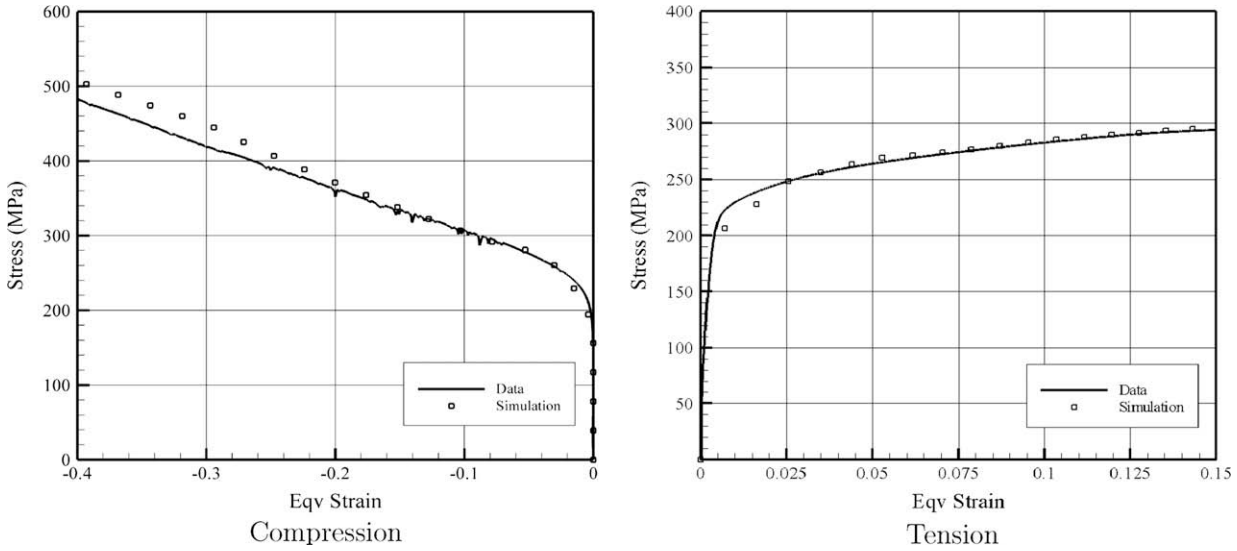

Fig. 18. Comparison between finite element simulation results using the proposed model and experimental data corresponding to uniaxial loading in the transverse direction. Symbols are simulation results.

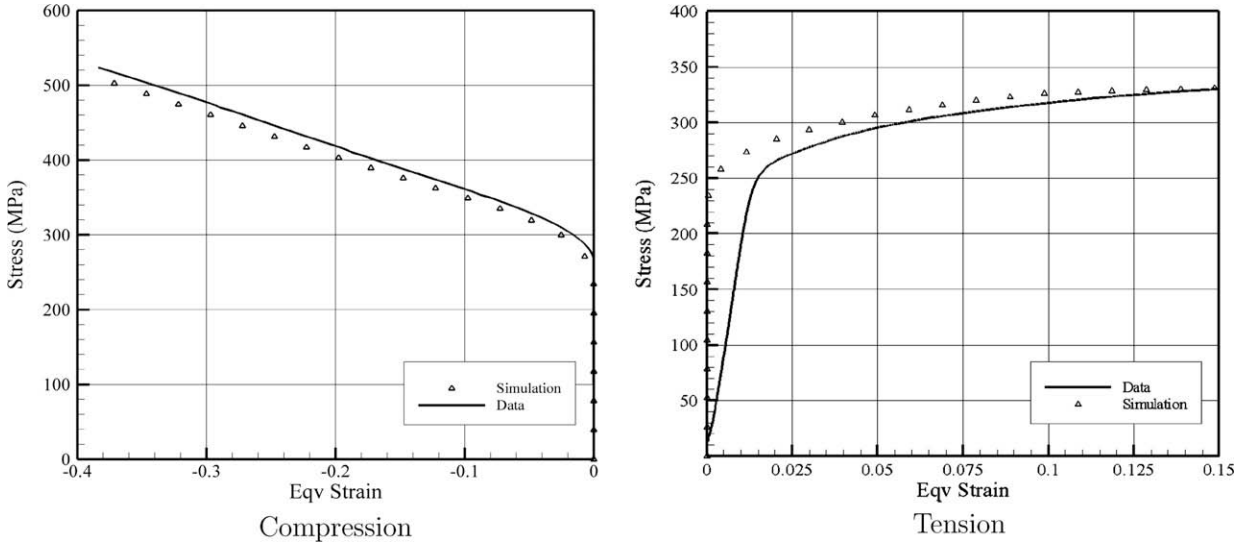

Fig. 19. Comparison between finite element simulation results using the proposed model and experimental data corresponding to uniaxial loading in the through thickness direction. Symbols are simulation results.

5. Concluding remarks

A comprehensive experimental and theoretical investigation of the deformation behavior of high-purity, polycrystalline α-titanium under quasi-static conditions at room temperature was conducted. To quantify the plastic anisotropy and the tension–compression asymmetry of this material monotonic tensile and compressive tests were conducted. The evolution of texture during deformation was studied using neutron-diffraction techniques to elucidate the role of deformation twinning and its effect on the macroscopic response.

From the test results, it can be concluded that the mechanical response is non-symmetric (tension–compression asymmetry) and orthotropic. Specifically, the hardening rate is strongly dependent on the loading direction and the sense of the applied load. The observed tension–compression asymmetry is a consequence of different deformation mechanisms being activated along different loading directions. The experimental evidence was further used to develop an elastic–plastic model. Key in its formulation is an anisotropic yield criterion that captures strength differential effects and an anisotropic hardening rule that accounts for texture evolution associated to twinning. The ability of the proposed model to capture

the main features of the observed behavior were assessed by comparing the experimental data with simulation results in terms of stress–strain response in uniaxial tensile and compression tests. A very good comparison between FE simulations using the model developed and uniaxial data was obtained.

In hexagonal materials SD (strength-differential) effects, which are due to the polarity of deformation twinning, are observed even for monotonic loadings. The aim of this paper was to describe the distortion of the yield surface associated with this tension–compression asymmetry. Future plans include modeling SD effects and hardening associated with cyclic loadings. It is expected that additional internal variables should be included in the present model such as a second order tensor to capture the backstress and a fourth-order tensor to capture twinning-detwinning effects under reverse loading. Note that such an approach was used by Teodosiu and co-workers (second-order tensor for description of backstress and fourth-order tensor for description of the polarity of dislocation walls) in conjunction with Hill (1948) yield criterion to model anisotropic hardening in materials with cubic crystal structure (see for example, Li et al., 2003). To model SD effects during cyclic loading observed in AZ31B Mg alloys, Lee et al. (2008) used Drucker–Prager compressible (pressure-dependent) yield criterion and a 2nd order internal variable to account for hardening evolution.

Acknowledgements

The texture measurements reported in this paper were conducted at Los Alamos Neutron Science Center (LANSCE) by Dr. Sven Vogel, whose help and input are gratefully acknowledged. O. Cazacu gratefully acknowledges the partial support for this work provided by US Air Force, Grant FA 8651-05-1-0005.

Appendix A. Derivatives of the yield function

Derivatives of the effective stress $\bar{\sigma}$ (see (5)) with respect to the Cauchy stress are provided in what follows. Applying the chain rule,

$$\frac{\partial\bar{\sigma}}{\partial\boldsymbol{\sigma}}=\frac{\partial\bar{\sigma}}{\partial J_2^\circ}\frac{\partial J_2^\circ}{\partial\boldsymbol{\Sigma}}\frac{\partial\boldsymbol{\Sigma}}{\partial\boldsymbol{\sigma}}+\frac{\partial\bar{\sigma}}{\partial J_3^\circ}\frac{\partial J_3^\circ}{\partial\boldsymbol{\Sigma}}\frac{\partial\boldsymbol{\Sigma}}{\partial\boldsymbol{\sigma}} \tag{A.1}$$

or

$$\frac{\partial\bar{\sigma}}{\partial\sigma_{ij}}=\frac{\partial\bar{\sigma}}{\partial J_2^\circ}\frac{\partial J_2^\circ}{\partial\Sigma_{kl}}\frac{\partial\Sigma_{kl}}{\partial\sigma_{ij}}+\frac{\partial\bar{\sigma}}{\partial J_3^\circ}\frac{\partial J_3^\circ}{\partial\Sigma_{kl}}\frac{\partial\Sigma_{kl}}{\partial\sigma_{ij}} \tag{A.2}$$

where

$$\frac{\partial\bar{\sigma}}{\partial J_2^\circ}=\frac{A_1^3(J_2^\circ)^{1/2}}{2\bar{\sigma}^2} \tag{A.3}$$

$$\frac{\partial\bar{\sigma}}{\partial J_3^\circ}=-\left(\frac{2c}{3}\right)\frac{A_1^3(J_3^\circ)}{\bar{\sigma}^2} \tag{A.4}$$

The derivatives of the generalized invariants with respect to the transformed stress $\boldsymbol{\Sigma}$ are

$$\frac{\partial J_2^\circ}{\partial\Sigma_{11}}=\Sigma_{11}\qquad\frac{\partial J_2^\circ}{\partial\Sigma_{22}}=\Sigma_{22}\qquad\frac{\partial J_2^\circ}{\partial\Sigma_{33}}=\Sigma_{33}$$
$$\frac{\partial J_2^\circ}{\partial\Sigma_{12}}=\Sigma_{12}\qquad\frac{\partial J_2^\circ}{\partial\Sigma_{13}}=\Sigma_{13}\qquad\frac{\partial J_3^\circ}{\partial\Sigma_{23}}=\Sigma_{23}$$
$$\frac{\partial\Sigma_{11}}{\partial\sigma_x}=\frac{1}{3}(a_2+a_3)\qquad\frac{\partial\Sigma_{22}}{\partial\sigma_x}=-\frac{1}{3}a_3\qquad\frac{\partial\Sigma_{33}}{\partial\sigma_x}=-\frac{1}{3}a_2$$
$$\frac{\partial\Sigma_{11}}{\partial\sigma_y}=-\frac{1}{3}a_3\qquad\frac{\partial\Sigma_{22}}{\partial\sigma_y}=\frac{1}{3}(a_1+a_3)\qquad\frac{\partial\Sigma_{33}}{\partial\sigma_y}=-\frac{1}{3}a_1$$
$$\frac{\partial\Sigma_{11}}{\partial\sigma_z}=-\frac{1}{3}a_2\qquad\frac{\partial\Sigma_{22}}{\partial\sigma_z}=-\frac{1}{3}a_1\qquad\frac{\partial\Sigma_{33}}{\partial\sigma_z}=\frac{1}{3}(a_1+a_2)$$
$$\frac{\partial\Sigma_{12}}{\partial\tau_{xy}}=a_4\qquad\frac{\partial\Sigma_{13}}{\partial\sigma_{xz}}=a_5\qquad\frac{\partial\Sigma_{23}}{\partial\sigma_{yz}}=a_6$$

All other derivatives are equal to zero.

References

Barlat, F., Cazacu, O., Zyczkowski, M., Banabic, D., Yoon, J., 2004. Yield surface plasticity and anisotropy in sheet metals. In: Raabe, D., Roters, F., Barlat, F., Chen, L.Q. (Eds.), Continuum Scale Simulation of Engineering Materials, Fundamentals – Microstructures – Process Applications. Wiley–VCH, Weinheim, Berlin GmbH, pp. 145–178.

Barlat, F., Yoon, J., Cazacu, O., 2007. On linear transformation-based anisotropic yield functions. International Journal of Plasticity 23, 876–896.

Cazacu, O., Barlat, F., 2001. Generalization of Drucker's yield criterion to orthotropy. Mathematics and Mechanics of Solids 6, 613–630.
Cazacu, O., Barlat, F., 2004. A criterion for description of anisotropy and yield differential effects in pressure-insensitive metals. International Journal of Plasticity 20, 2027–2045.
Cazacu, O., Barlat, F., 2008. Modeling plastic anisotropy and strength differential effects in metallic materials. In: Cazacu, O. (Ed.), Multiscale Modeling of Heterogeneous Materials: From Microstructure to Macro-Scale Properties. ISTE Ltd. and Wiley Inc., New York, pp. 71–87.
Cazacu, O., Plunkett, B., Barlat, F., 2006. Orthotropic yield criterion for hexagonal closed packed metals. International Journal of Plasticity 22, 1171–1194.
Chun, Y.B., Yu, S.L., Semiatin, S.L., Hwang, S.K., 2005. Effect of deformation twinning on microstructure and texture evolution during cold rolling of cp-titanium. Materials Science and Engineering A 398, 209–219.
Follansbee, P.S., Gray, G., Wu, P.D., 1989. An analysis of the low temperature, low and high strain-rate deformation of Ti–6Al–4V. Metallurgical Transactions A 20, 863–874.
Graff, S., Brocks, W., Steglich, D., 2007. Yielding of magnesium: from single crystal to polycrystalline aggregates. International Journal of Plasticity 23, 1957–1978.
Hill, R., 1948. A theory of the yielding and plastic flow of anisotropic metals. Proceedings of the Royal Society of London A 193, 281–297.
Hosford, W., 2005. Mechanical Behavior of Materials. Cambridge University Press, Cambridge.
Hosford, W.F., Allen, T., 1968. Deformation characteristics of textured magnesium. Transactions of the TMS-AIME 242, 654–661.
Hosford, W.F., Allen, T., 1973. Twinning and directional slip as a cause for a strength differential effect. Metallurgical Transactions 4, 1424–1425.
Johnson, G.R., Beissel, S.R., Stryk, R.A., Gerlach, C.A., Holmquist, T.J., October 2003. User instructions for the 2003 version of the EPIC code. Tech. Rep., Network Computing Services Inc., Minneapolis, MN.
Kaschner, G.C., Lovato, M.L., Stout, M.G., Proust, G., Liu, C., Beyerlein, I.J., Usov, I., Wang, Y., Tome, C.N., in press. Mini-tensile experiments of clock-rolled zirconium plate. Experimental Mechanics, doi:10.1007/s11340-008-9213-6.
Khan, A., Suh, Y., Kazmi, R., 2004. Quasi-static and dynamic loading responses and constitutive modeling of titanium alloys. International Journal of Plasticity 20, 2233–2248.
Khan, A., Kazmi, R., Farroch, B., 2007. Multiaxial and non-proportional loading responses, anisotropy and modeling of Ti–6Al–4V titanium alloy over wide ranges of strain rates and temperatures. International Journal of Plasticity 23, 931–950.
Kuwabara, T., Katami, C., Kikuchi, M., Shindo, T., Ohwue, T., 18–20 June 2001. Cup drawing of pure titanium sheet – finite element analysis and experimental validation. In: Proceedings of the Seventh International Conference on Numerical Methods in Industrial Forming Processes, Toyohashi, Japan. pp. 781–787.
Lee, D., Backofen, W.A., 1966. Yielding and plastic deformation in textured shett of titanium and its alloys. Transactions of the TMS-AIME 236, 1703–1966.
Lee, W.S., Lin, M., 1997. The effects of strain rate and temperature on the compressive deformation behavior of Ti–6Al–4V alloy. Journal of Materials Processing Technology 71, 235–246.
Lee, M.-G., Wagoner, R., Lee, J., Chung, K., Kim, H., 2008. Constitutive modeling for anisotropic/asymmetric hardening behavior of magnesium alloy sheets. International Journal of Plasticity 24, 545–582.
Li, Q., Xu, Y., Bassim, M.N., 1997. Dynamic mechanical behavior of pure titanium. Journal of Materials Processing Technology 155, 1889–1892.
Li, S., Hoferlin, E., Bael, A.V., Houtte, P.V., Teodosiu, C., 2003. Finite-element modeling of plastic anisotropy induced by texture and strain-path changes. International Journal of Plasticity 19, 647–674.
Lou, X., Li, M., Boger, R., Agnew, S., Wagoner, R., 1997. Hardening evolution of AZ31B Mg sheet. International Journal of Plasticity 23, 44–86.
Nemat-Nasser, S., Guo, W.-G., Nesterenko, V., Indrakanti, S., Gu, Y.-B., 2001. Dynamic response of conventional and hot isostatically pressed Ti–6Al–4V alloys: experiments and modeling. Mechanics of Materials 33, 425–439.
Picu, R., Majorell, A., 2002. Mechanical behavior of Ti–6Al–4V at high and moderate temperatures. Part II: constitutive modeling. Materials Science and Engineering A 326, 306–316.
Plunkett, B., Cazacu, O., 2008. Viscoplastic modeling of anisotropic textured metals. In: Cazacu, O. (Ed.), Multiscale Modeling of Heterogeneous Materials: From Microstructure to Macro-Scale Properties. ISTE Ltd. and Wiley Inc., New York, pp. 111–126.
Plunkett, B., Lebensohn, R.A., Cazacu, O., Barlat, F., 2006. Evolving yield function of hexagonal materials taking into account texture development and anisotropic hardening. Acta Materialia 54, 4159–4169.
Proust, G., Tome, C.N., Kaschner, G.C., 2007. Modeling texture, twinning, and hardening evolution during deformation of hexagonal materials. Acta Materialia 55, 2137–2148.
Salem, A.A., Kalidindi, S.R., Doherty, R.D., 2003. Strain hardening of titanium: role of deformation twinning. Acta Materialia 51, 4225–4237.
Simo, J., Hughes, T., 1998. Computational Inelasticity. Springer, New York.
Staroselsky, A., Anand, L., 2003. A constitutive model for hcp metals deforming by slip and twinning: application to magnesium alloy AZ31. International Journal of Plasticity 19, 1843–1864.
Tome, C.N., Lebensohn, R.A., 2004. Self-consistent homogenization methods for texture and anisotropy. In: Raabe, D., Roters, F., Barlat, F., Chen, L.-Q. (Eds.), Continuum Scale Simulation of Engineering Materials, Fundamentals – Microstructures - Process Applications. Wiley–VCH, Berlin GmbH, pp. 473–497.
Tome, C.N., Maudlin, P.J., Lebensohn, R.A., Kaschner, G.C., 2001. Mechanical response of zirconium: I. Derivation of a polycrystal constitutive law and finite element analysis. Acta Materialia 49, 3085–3096.
Vitek, V., Mrovec, M., Bassani, J.L., 2004. Influence of non-glide stresses on plastic flow: from atomistic to continuum modeling. Materials Science and Engineering A 365, 31–37.
Wu, X., Kalidindi, S.R., Necker, C., Salem, A., 2007. Prediction of crystallographic texture evolution and anisotropic stress–strain curves during large plastic strains in high purity α-titanium using a Taylor-type crystal plasticity model. Acta Materialia 55, 423–432.